Published in final edited form as:
Alzheimer Dis Assoc Disord. 2013 January ; 27(1): 74–83. doi:10.1097/WAD.0b013e31824a7df4.

Patterns of striatal degeneration in frontotemporal dementia

Cathra Halabi, B.S.[a], **Anasheh Halabi, B.S.**[a], **David L. Dean, B.S.**[a], **Pei-Ning Wang, M.D., Ph.D.**[b], **Adam L. Boxer, M.D., Ph.D.**[a], **John Q. Trojanowski, M.D., Ph.D.**[c], **Stephen J. DeArmond, M.D., Ph.D.**[d], **Bruce L. Miller, M.D.**[a], **Joel H. Kramer, Psy.D.**[a], and **William W. Seeley, M.D.**[a,*]

[a]Department of Neurology, University of California, San Francisco

[b]Department of Neurology, National Yang-Ming University, School of Medicine and Taipei Veterans General Hospital, Taipei, Taiwan

[c]Department of Pathology, University of Pennsylvania

[d]Department of Pathology, University of California, San Francisco

Abstract

Behavioral variant frontotemporal dementia and semantic dementia have been associated with striatal degeneration, but few studies have delineated striatal subregion volumes *in vivo* or related them to clinical phenotype. We traced caudate, putamen, and nucleus accumbens on MR images to quantify volumes of these structures in behavioral variant frontotemporal dementia, semantic dementia, Alzheimer's disease, and healthy controls (n = 12 per group). We further related these striatal volumes to clinical deficits and neuropathological findings in a subset of patients. Behavioral variant frontotemporal dementia and semantic dementia showed significant overall striatal atrophy compared with controls. Moreover, behavioral variant frontotemporal dementia showed panstriatal degeneration whereas semantic dementia featured a more focal pattern involving putamen and accumbens. Right-sided striatal atrophy, especially in the putamen, correlated with overall behavioral symptom severity and with specific behavioral domains. At autopsy, patients with behavioral variant frontotemporal dementia and semantic dementia showed striking and severe tau or TAR DNA-binding protein of 43 kDa pathology, especially in ventral parts of the striatum. These results demonstrate that ventral striatum degeneration is a prominent shared feature in behavioral variant frontotemporal dementia and semantic dementia and may contribute to social-emotional deficits common to both disorders.

1. Introduction

Frontotemporal dementia (FTD) describes a group of clinical syndromes united by underlying frontotemporal lobar degeneration (FTLD) pathology. Consistent with this nomenclature, FTD has long been associated with focal cortical atrophy, whereas subcortical structures have received less emphasis. In the behavioral variant of FTD (bvFTD) and semantic dementia (SD), however, dramatic changes in eating, sexual conduct, and compulsivity emerge, all of which may relate to striatal dysfunction[1–6]. Later-stage patients often show extrapyramidal motor signs, such as rigidity and bradykinesia, which may reflect a loss of nigrostriatal projection targets[7]. Considering recent functional imaging evidence that neurodegenerative syndromes cause atrophy within functionally interconnected neural systems[8], the specific subcortical regions affected by the canonical cortical dementias merit further exploration.

*Correspondence to: William W. Seeley, M.D., Department of Neurology, University of California, San Francisco, 350 Parnassus, Suite 905, San Francisco, CA 94143-1207, Phone: 415-476-6880 Fax: 415-476-4800, wseeley@memory.ucsf.edu.

Previous work on FTD-related striatal involvement has been limited by methodological factors or project scope, and no study has assessed all striatal subregions at once using manual volumetric methods. Some voxel-based morphometry (VBM) studies[9–12] and other automated imaging analyses[13, 14] have emphasized striatal disease, but VBM may overestimate striatal atrophy due to spatial misregistration near the ventricles[15]. Previous work from our group[16] used manual region-of-interest (ROI) tracings to confirm caudate and putamen atrophy detected by VBM in a small group of pathologically diagnosed FTLD patients. Manual ROI tracing studies further showed caudate[17] and putamen[18] atrophy in FTD subtypes but did not relate subregion volumes to behavior, histopathology, or each other, and there is no quantitative data available regarding nucleus accumbens volume. Studies of abnormal eating[1, 19] and motor stereotypies[20] have used VBM to link striatal atrophy to behavior but did not resolve subregion-specific correlations. Patients with bvFTD often show marked striatal degeneration at autopsy, but few studies have characterized post-mortem striatal volume loss[21] or histopathology[22–24], and pathological studies can rarely shed light on early-stage disease. In SD, an anterior temporal disease, striatal injury remains minimally studied despite robust connections between the temporal pole and ventral striatum in the healthy brain[14, 25, 26].

Current FTLD pathological nomenclature is based on the protein composition of neuronal and glial inclusions, with most patients showing either tau (FTLD-tau) or transactive response DNA-binding protein of 43 kDa (TDP-43, FTLD-TDP) immunoreactive inclusions, and a small proportion showing fused in sarcoma (FUS) immunoreactive inclusions only (FTLD-FUS)[27, 28]. Patients with bvFTD are divided evenly among FTLD-tau and FTLD-TDP, whereas most with SD show FTLD-TDP pathology, Type C[29], characterized by a lack of cortical neuronal cytoplasmic inclusions (NCIs) in favor of long, swollen dystrophic neurites (DNs) in superifical layers[22, 30, 31]. Interestingly, a survey of subcortical pathology in FTLD-TDP[22] described Pick body-like putaminal NCIs in SD (FTLD-TDP, Type 1, now referred to as Type C), suggesting that NCIs may be more prevalent in this subtype than previously recognized and restricted to subcortical structures.

We sought to fill a lingering gap in the literature by determining specific patterns of caudate, putamen, and nucleus accumbens (NAcc) atrophy in bvFTD and SD compared to healthy controls (HC) and Alzheimer's disease (AD). Based on the concept of network-based neurodegeneration[8] and known patterns of cortico-striatal connectivity[25], we hypothesized that bvFTD would be associated with panstriatal injury, while SD would show a more ventral pattern with prominent NAcc degeneration. In patients for whom behavioral data were available, we explored the relationship between behavioral symptoms and striatal subregion volumes, predicting that reward-related behaviors, such as aberrant motor behaviors and eating disorder, would correlate with NAcc atrophy. Finally, to generate hypotheses regarding the mechanisms of striatal injury, we examined neuropathological materials from selected patients with FTLD who had undergone autopsy.

2. METHODS

2.1. Subjects

Forty-eight subjects were selected from the University of California at San Francisco (UCSF) Memory and Aging Center database. Subjects belonged to the following groups: HC (n = 12), probable AD (n = 12), bvFTD (n = 12), and SD (n = 12). All subjects were evaluated by a multi-disciplinary team that included a neurologist, neuropsychologist, and a nurse and were reviewed at a consensus conference as described previously[32]. Patients were diagnosed according to consensus clinical diagnostic criteria[33, 34]. For SD, patients with both left- (n = 8) and right- (n = 4) temporal predominant presentations[4] were included, as long as they met research criteria for SD. In keeping with research criteria for all groups, no

specific MRI atrophy pattern was required for diagnosis. Healthy control subjects were recruited community-dwelling volunteers who lacked a neurological or psychiatric history, structural disease on MRI, or a Clinical Dementia Rating (CDR) scale score greater than zero.

Subject selection proceeded as follows. Because fewer bvFTD and SD subjects were available in the database at the time of sample selection, these subjects were identified first, based on availability of a high quality 1.5 Tesla MRI scan obtained within three months of diagnosis. Forty-five bvFTD and 19 SD subjects met these entry criteria at the time of group selection. From these pools, 12 bvFTD and 12 SD subjects were matched to each other, as closely as possible, for age, gender, and education. Patients with available neuropsychological, behavioral, and motor data were included whenever possible within matching constraints. To limit disease severity effects on group differences, we further matched for Mini Mental State Examination (MMSE). Next, we selected 12 patients with probable AD and 12 HC subjects to match the bvFTD and SD groups, again using age, gender, education, and MMSE (for AD only). Group demographic and neuropsychological variables are shown in Table 1. As a result of the matching procedure, groups did not significantly differ in age, gender, or education. In addition, patient groups did not significantly differ in MMSE, CDR, or disease duration (Table 1).

All subjects or their surrogates provided informed consent, and the study was approved by the UCSF Committee on Human Research.

2.2. MRI acquisition and pre-processing

MRI scans were obtained on a 1.5T MR scanner (Siemens Inc., Iselin, NJ) equipped with a standard quadrature head coil. Structural MRI sequences, detailed previously[9], were chosen to obtain proton density, T1-weighted, and T2-weighted images, covering the entire brain. The T1-weighted images used as the primary basis for tracing were obtained using a volumetric magnetization prepared rapid gradient echo MRI (repetition time/echo time/inversion time = 10/4/300 milliseconds), 15° flip angle, coronal orientation perpendicular to the double spin echo sequence, 1.0 × 1.0 mm2 in-plane resolution, and 1.5-mm slab thickness.

MRIs were analyzed on a Linux workstation using the BRAINS2 software package. BRAINS2 is developed and made freely available by the Mental Health–Clinical Research Center at the University of Iowa[35]. The T1-weighted images were resampled to 1.0-mm^3 voxels and spatially realigned so that the anterior–posterior axis of the brain was realigned parallel to the anterior commissure-posterior commissure line and the interhemispheric fissure was aligned with the other two orthogonal axes. The Talairach grid[36] was warped onto the resampled and spatially realigned T1-weighted images by using the outermost boundaries of the cortex, the anterior commissure, and the posterior commissure as landmarks. The T2- and proton density–weighted images were then realigned to the T1-weighted image with an automated image registration program[37].

A discriminant analysis method based on automated training class selection[38] was applied to the coregistered images to resample images into gray matter, white matter, and cerebrospinal fluid. This tissue classification algorithm uses a Bayesian classifier based on discriminant analysis to reduce the variability in signal intensity across individual image sets and to correct for partial volume effects. This step requires the manual tracing of venous blood but is able to perform “plug” selection for gray matter, white matter, and cerebrospinal fluid. The resulting segmented image was used to facilitate manual ROI tracing, but the boundaries of the ROIs suggested by these images were not considered equivalent to the spatial extent of the ROIs. Instead, ROIs were traced according to standardized anatomic

landmarks, as described below. Finally, we generated a brain mask using a previously trained artificial neural network, a feature of the BRAINS2 software package. An automated Talairach-based method of regional classification was used to calculate lobar volumes[35]. Total cerebral volume (TCV) was assessed by summing frontal, temporal, parietal, and occipital lobar volumes. Total intracranial volume (TIV) was calculated as the sum of the volumes from all three tissue compartments within a separate mask of all intracranial contents.

2.3. ROI tracing and volume measurement

A single investigator (C.H.) blinded to all clinical and pathological information manually traced caudate, putamen, and NAcc ROIs on MR images of all 48 subjects. This investigator was trained extensively before data collection began by tracing regions of interest for subjects not included in the study. These trial runs were reviewed by a neurologist with neuroimaging and anatomical expertise (W.W.S.) to identify tracing errors and make appropriate adjustments. After training was completed, experimental tracings began, and reliability assessments were incorporated as described below.

All tracings were performed with three orthogonal planes in view. T1 and T2-weighted images were superimposed on segmented images to allow toggling between images that facilitated landmark identification. ROI tracing was performed directly on T1-weighted coronal images and proceeded from anterior to posterior. Structures in the left hemisphere were drawn first for each subject. Subregions were traced using the following anatomical boundaries: (1) Caudate: anterior = termination of the caudate head; medial = frontal horn of the lateral ventricle; lateral = internal capsule; inferior = the genu of the corpus callosum or, more posteriorly, the NAcc; posterior = tail of the caudate no longer visible or curves inferoposteriorly past the thalamus; (2) Putamen: anterior = initial bifurcation of striatal mass by internal capsule; medial = NAcc and the anterior limb of internal capsule (anteriorly) or globus pallidus and genu of internal capsule (posteriorly); lateral = external capsule (care was taken to exclude the claustrum when visible); superior and inferior = surrounding white matter; posterior = putamen no longer visible; (3) NAcc: anterior = posterior portion of ventral caudate head, where T1 hypointense signal contour begins; medial = white matter superior to posterior orbital cortex; lateral = anterior limb of internal capsule, or, more posteriorly, the putamen; inferior = continuation of pre-orbital white matter; posterior = emergence of anterior commissure. Group-representative tracings and 3D ROI reconstructions are shown in Figure 1A, which features the first subject whose total striatal volume was above their diagnostic group median. Areas outlined by each ROI tracing were multiplied by the slice thickness to yield an ROI volume for that scan, and resulting volumes were summed to yield a total volume for each structure in cubic centimeters (cc). We elected not to trace globus pallidus or thalamus because the boundaries of these structures could not be reliably visualized on our MR images.

2.4. Reliability

To assess intra-rater reliability, CH re-traced all ROIs for four randomly selected subjects (3 bvFTD, 1 control; interval between original tracings and reliability tracings ranged from 15 to 19 months). The goal of this intra-rater assessment was to assess the degree of rater drift throughout the experiment. Although only CH's original tracings were used for study-related hypothesis testing, to determine the reproducibility of our tracing methods, we also assessed inter-rater reliability by having a second similarly trained investigator (AH) trace the same four scans used for the intra-rater assessment. For intra-rater reliability, intraclass correlation coefficients (ICCs, consistency model) ranged from 0.78 to 0.91 (left caudate = 0.79, left putamen = 0.91, left NAcc = 0.91; right caudate = 0.79, right putamen = 0.90, right NAcc = 0.78). These reliability data, which characterize the rater who performed all tracings

used for hypothesis testing, suggest that intra-rater drift throughout the experiment was mild. Inter-rater reliability was generally high, with ICCs (absolute agreement model) ranging from 0.66 to 0.96 (left caudate =0.96, left putamen = 0.95, left NAcc = 0.93; right caudate = 0.90, right putamen = 0.91, right NAcc = 0.66). Because right NAcc inter-rater reliability was lower than seen for any other region, we performed a third analysis to assess agreement across all three right NAcc measurements (original, intra-rater, and inter-rater). This ICC (absolute agreement model) was 0.80, suggesting that our methods for assessing right NAcc volume produce acceptable overall reliability. All statistical analyses were implemented in SPSS 15.0 software (SPSS Inc., Chicago, IL).

2.5. Motoric and behavioral assessment

A subset of 21 patients (6 AD, 7 bvFTD, 8 SD) had a standardized prospectively recorded neurological examination in the database. From this dataset, we extracted the 10 items relating to parkinsonian signs (facial expression (0–4), rest tremor (0–4), postural tremor (0–4), rigidity (0–4), posture (0–4), gait (0–4), body bradykinesia (0–4), cogwheeling (0–3), reduced armswing (0–3), dyskinesia (0–3)), as well as 2 items relating to the presence of myoclonus (0–3) or disrupted Luria hand motor sequences (0–4). We then derived total scores for the motor examination (maximum = 44, with higher scores indicating greater deficits) for correlation with regional volumes. NPI data were available for 22 patients (7 AD, 8 bvFTD, 7 SD). We selected euphoria, apathy, disinhibition, aberrant motor, and eating subscales, as well as the NPI total score (frequency x severity products), because these measures best capture the bvFTD and SD behavioral profile[32].

2.6. Neuropathology

Although patients were selected based solely on clinical syndrome, neuropathological diagnoses were or became available for 7 AD, 9 bvFTD, 6 SD subjects. Autopsies were performed at University of Pennsylvania, UCSF, or the University of Southern California (one patient) using standard dementia protocols described previously[16]. Pathological FTLD and AD were diagnosed according to current consensus criteria[28, 39], and FTLD-TDP subtyping followed the recently harmonized lettering scheme[29]. All 7 patients with clinical AD had high likelihood AD at autopsy, 1 with co-morbid Lewy body pathology (diffuse neocortical type). In the bvFTD group, four patients had Pick's disease; one had corticobasal degeneration (CBD); one had FTLD-TDP, Type A; one had FTLD-TDP, Type B; one had high likelihood AD; and one had FTLD with fused in sarcoma (FUS) immunoreactive inclusions, the atypical FTLD-U subtype[27]. In the SD group, five patients had FTLD-TDP Type C, and one patient had FTLD with tau-negative, ubiquitin-positive intraneuronal inclusions (FTLD-U) that were not characterized (using TDP-43 or FUS immunohistochemistry) or subtyped according to pathomorphology and laminar distribution[29].

Having identified striatal atrophy in patients with bvFTD and SD, we explored striatal histopathological features among patients neuropathologically evaluated at UCSF, including two with bvFTD (one with CBD, one with FTLD-TDP, Type A) and four with SD (all with FTLD-TDP, Type C). Relevant eight micron-thick, paraffin-embedded fixed tissue sections were immunostained for hyperphosphoryated tau (CP13 antibody, courtesy of Peter Davies), ubiquitin (anti-rabbit, 1:1000, DAKO North America, Carpinteria, CA), or TDP-43 (anti-rabbit, 1:2000, Proteintech Group, Chicago, IL) as appropriate and were examined qualitatively for the abundance and distribution of NCIs, DNs, neuronal intranuclear inclusions (NIIs) and glial cytoplasmic inclusions (GCIs).

2.7. Statistical methods

Demographic and neuropsychological variables were compared across groups using one-way analysis of variance (ANOVA), with post hoc Tukey tests for pairwise comparisons, or chi-square tests, as appropriate (Table 1). To assess the effect of diagnostic group on each striatal subregion, we used repeated measures ANOVA, treating each subregion volume as a single dependent variable, with side (left or right) as the within-subjects factor and diagnosis as the between-subjects factor. Total intracranial volume (TIV) was entered as a covariate, and a post hoc Bonferroni correction for pairwise multiple comparisons was applied. To determine whether between-group differences in striatal subregion atrophy could be attributed to overall brain atrophy, we repeated the primary analyses after adding TCV as a covariate. For clarity, we used TIV-corrected group-level striatal subregion volumes to calculate group percentage differences (Results) and for illustration (Figure 1B).

Correlations between left and right subregion volumes were examined using partial correlation, controlling for age, gender, and TIV. We further assessed relationships between ROI volumes and the NPI (patients only, examining behavioral subscales and the total score as described above) using partial correlations (one-tailed), first controlling for TIV only and correcting for multiple comparisons using the Bonferroni method. Correlations significant at the Bonferroni-corrected threshold were then re-analyzed controlling for TIV and diagnosis (coded using dummy variables that represented the three patient groups) to determine whether the observed behavioral correlations were attributable to diagnostic group membership. Finally, in a similar fashion, we controlled for TIV, diagnosis and TCV. For the analyses in which diagnosis and TCV were included, we accepted a statistical significance of $p < 0.05$. To evaluate the relationship between striatal ROI volumes and motor deficits, we used Spearman correlations (one-tailed) because the motor exam scores were non-normally distributed. Therefore, we corrected the striatal subregion volumes for TIV by multiplying each volume by the ratio of the overall sample mean TIV and the subject's TIV. One-tailed tests were used for the behavioral and motor correlations because only an inverse relationship between volume and symptom severity was considered biologically plausible.

3. RESULTS

3.1.1. Group differences in striatal volumes—Examining the impact of diagnostic group on total and subregional striatal volume, we found a significant main effect of diagnosis on total striatal volume ($F = 9.33$, $p = 0.00007$) and for all three subregions, including caudate ($F = 7.48$, $p = 0.0004$), putamen ($F = 7.48$, $p = 0.0004$), and NAcc ($F = 10.45$, $p = 0.00003$). In Figure 1B, TIV-corrected volume means are displayed for each subregion to highlight the results of the posthoc pairwise comparisons, detailed in the following four sections.

3.1.2. Total striatum—Patients with bvFTD (TIV-corrected mean total striatal volume = 5.89 cc, s.d. = 1.58) had 25% lower total striatal volume than HC (mean = 7.81 cc, s.d. = 0.81, $p = 0.0002$) and 20% lower total striatal volumes than AD (mean = 7.39 cc, s.d. = 0.62, $p = 0.003$). Patients with SD (mean = 6.34 cc, s.d. = 1.05) had 19% lower total striatal volumes than HC ($p = 0.009$) but did not differ from those with AD ($p = 0.1$). No difference in total striatal volume between bvFTD and SD was detected, nor was an overall interaction between diagnostic group and side ($F = 0.87$, $p = 0.47$).

3.1.3. Caudate—Patients with bvFTD (TIV-corrected mean caudate volume = 2.81 cc, s.d. = 0.79) had 20% lower caudate volumes than HC (mean = 3.5 cc, s.d. = 0.47, $p = 0.01$) and 23% lower volumes than AD (mean = 3.67 cc, s.d. = 0.39, $p = 0.001$), whereas patients with

SD (mean = 3, s.d. = 0.52) had 18% lower volumes than AD (p = 0.02) but did not differ significantly from controls. AD showed no caudate atrophy compared to controls (p = 1.0). There were no group differences in caudate volume between bvFTD and SD, and there was no overall interaction between diagnostic group and side (F = 0.77, p = 0.52).

3.1.4. Putamen—Patients with bvFTD (TIV-corrected mean putamen volume = 2.88 cc, s.d. = 0.82) had 28% lower putaminal volumes than HC (mean = 3.97 cc, s.d. 0.54, p = 0.0003), and patients with SD (mean = 3.15, s.d. = 0.59) had 21% lower volumes than HC (p = 0.01). AD putaminal volumes (mean = 3.46 cc, s.d. 0.40) did not show significant atrophy compared to HC (p = 0.3) nor did they differ from bvFTD (p = 0.1) or SD (p = 1). There were no differences in putaminal volumes between bvFTD and SD, and there was no interaction between diagnostic group and hemisphere (F = 0.54, p = 0.66).

3.1.5. Nucleus Accumbens—Patients with bvFTD (TIV-corrected mean NAcc volume = 0.21 cc, s.d. = 0.08) had 40% lower NAcc volumes than HC (mean = 0.35 cc, s.d. = 0.07, p = 0.0002), and patients with SD (mean = 0.19 cc, s.d. = 0.07) had 44% lower volumes than HC (p = 0.00006). AD (mean = 0.26 cc, s.d. 0.08) showed a trend toward NAcc atrophy compared to HC that did not reach statistical significance (p = 0.06). There were no group differences in NAcc volumes between AD, bvFTD, and SD, but there was a significant interaction between diagnostic group and hemisphere (F = 5.55, p = 0.003), with bvFTD showing smaller right-sided NAcc volumes and SD showing smaller left-sided NAcc volumes.

3.2. Striatal volume losses exhibit high interhemispheric correlation and cannot be attributed to cortical volume loss alone

As shown in Figure 2, left and right hemisphere striatal subregion volumes were highly correlated with each other (caudate r = 0.78, putamen r = 0.87, NAcc r = 0.86; all $p < 0.001$). To determine whether striatal atrophy in bvFTD and SD merely reflected overall cortical volume loss, we repeated each analysis presented in the preceding section including TCV as a covariate. Total striatum volumes remained significantly atrophied in bvFTD compared to AD (p = 0.03), and caudate volumes remained significantly atrophied in bvFTD (p = 0.01) and SD compared to AD (p = 0.02). Putamen and NAcc volumes no longer showed significant group differences after correcting for TCV. Together, these findings suggest that striatal volume loss in FTD cannot be attributed to cortical atrophy alone, especially in the caudate nucleus, but that the cortex and striatum may also co-degenerate in FTD, especially within ventral cortico-striatal networks.

3.3. Striatal atrophy correlates with behavioral but not motor deficits

Correlations between striatal subregion volumes and behavior are detailed in Table 2 and summarized here. Although several striatum-NPI relationships of interest were identified in exploratory analyses not corrected for multiple comparisons (Table 2), right putamen and right total striatal volumes each remained significantly correlated with aberrant motor behavior and NPI total after correction. These correlations remained significant at the $p < 0.05$ level after further controlling for diagnosis, and the correlation between right putaminal volume and aberrant motor behavior remained after controlling for both diagnosis and TCV.

Patient groups did not differ significantly on the total motor exam score (AD mean = 4.7, s.d. = 2.7, n = 6; bvFTD mean = 8.0, s.d. = 7.8, n = 7; SD mean = 2.3, s.d. = 2.0, n = 8), and there were no significant correlations across groups (n = 21) between total motor exam scores and striatal volumes (total striatum, Spearman $\rho = 0.08$, p = 0.37; caudate, Spearman $\rho = 0.20$, p = 0.18; putamen, Spearman $\rho = -0.04$, p = 0.44; NAcc, Spearman $\rho = 0.12$, p = 0.30).

3.8. Relationships between striatal atrophy and neuropathology

Although this study was designed to assess striatal atrophy in clinically defined syndromes, neuropathological diagnoses became available for 22 of 36 patients. These data (Figure 2) example, a patient with AD associated with a presenilin-1 mutation showed low striatal volumes compared to the rest of the AD group. Across the bvFTD-associated pathological spectrum, the most severe striatal atrophy was seen in the patient with FTLD-FUS.

Selected patients with FTLD-tau and FTLD-TDP pathology were examined to explore the pattern of striatal histopathology. Neuron loss, astrogliosis, and focal microvacuolation, especially in ventral striatal regions, were accompanied by robust tau or TDP-43 immunoreactive NCIs and DNs. Strikingly, abundant round, circumscribed TDP-43 immunoreactive NCIs were observed in all patients with SD due to FTLD-TDP, Type C (Figure 3). These large, round, circumscribed NCIs, recently identified in the putamen[22], were focally accentuated in the NAcc and contrast with the sparse cortical NCIs associated with this FTLD-TDP subtype.

4. Discussion

Although previous neuroimaging[7, 9–12, 17, 18, 40, 41] and histopathological studies[21–23] have noted general striatal involvement in FTD, this study provides a systematic investigation of striatal subregion atrophy in early bvFTD, SD, and AD. By focusing on specific striatal subregions and using manual volumetric methods better suited to delineate and quantify these structures, we identified pan-striatal atrophy in bvFTD and more selective putamen and NAcc atrophy in SD. Severe NAcc degeneration in bvFTD and SD was the most striking and novel finding, in part because previous studies were not designed to assess this subregion. Ventral striatal atrophy correlated with behavioral but not motor deficits and was associated with severe neurodegeneration featuring abundant tau or TDP-43 immunoreactive NCIs, most strikingly in SD due to FTLD-TDP Type C. Importantly, overall striatal atrophy was not explained by cortical volume loss alone and was less prominent or absent in patients with AD compared to controls.

4.1. Impact of striatal atrophy on behavior

Social, emotional, and behavioral changes represent shared features among patients with bvFTD and SD[3, 32, 42]. Many of these symptoms could relate to striatal or corticostriatal network impairment. The ventral striatum forms a critical node in the dopamine reward system[43], whose dysfunction in bvFTD and SD may manifest as disinhibited sexual behaviors; food cravings or aversions, changes in substance abuse patterns, and repetitive or compulsive behaviors[2, 4–6]. Although these symptoms also reflect medial frontal and frontoinsular cortex atrophy common to bvFTD and SD[9, 44], several recent studies suggest striatal correlations with symptom severity. Gluttonous overeating, for example, correlates with right-sided frontoinsular but also right striatal degeneration[1, 19]. Some aberrant motor behaviors, particularly motor stereotypies and hoarding, may reflect striatal involvement[20, 41]. Still, because these previous studies used VBM to quantify striatal volume, subregion localization has not been available. Here, subregional and total striatal atrophy measures were associated with behavioral deficits, even after accounting for overall cortical atrophy. Dysfunctional eating showed the most subregion-specific relationship, correlating only with right hemisphere NAcc volume. Although consistent with a previous study[1], this association did not survive a stringent multiple comparisons correction. Aberrant motor behavior, which in bvFTD and SD most often takes the form of repetitive and compulsive actions, correlated with right-sided striatal degeneration, especially involving the putamen. Overall, our behavioral correlations converge with prior work to suggest that reward-related FTD symptoms reflect right-lateralized ventral striatal circuit dysfunction,

especially involving the NAcc and putamen. Extrapyramidal motor deficits, in contrast, showed no correlations with any striatal subregion, most likely because the cortico-striatal networks first targeted in bvFTD and SD reflect socio-behavioral rather than motor systems. Furthermore, the early-stage patients included in this study had relatively few motor deficits, which may arise later as nigrostriatal dopaminergic inputs falter[7].

4.2. Neuropathological correlates of striatal degeneration

Abundant striatal tau pathology, manifesting as NCIs, DNs, GCIs, and white matter threads, has been widely reported in patients with FTLD-tau[23]. In this study, we found severe NAcc atrophy in SD, which rarely results from FTLD-tau[31, 45, 46], and we explored this finding in available neuropathological materials. Patients with SD due to FTLD-TDP, Type C showed severe striatal degeneration with conspicuous TDP-43 immunoreactive NCIs, especially in ventral striatum, accompanied by few DNs coursing through the surrounding neuropil. These findings complement a recent analysis of subcortical pathology in FTLD-TDP[22], in which similar though perhaps less abundant NCIs were described in the putamen. Large-scale regional mapping of TDP-43 pathology further suggested prominent striatal involvement, especially in patients with Type C[24]. Thus, in FTLD-TDP, Type C, the striatum contrasts with the cortex, which shows few NCIs but prominent long, swollen DNs[30]. Future studies could explore interactions between striatal NCIs and region-specific cortical DNs in patients with SD.

Notably, among patients with pathological AD, lower ventral striatal volumes were associated with a bvFTD clinical presentation, comorbid DLB, or a presenilin-1 mutation. These preliminary observations suggest that striatal atrophy in AD may often relate to atypical disease features. Recent studies suggest that amyloid deposition in presenilin-1-associated AD begins in the striatum[47], and the atrophy seen in the patient reported here suggests that this early involvement has degenerative consequences. Our data do not suggest, however, that preserved striatal volume alone could predict AD pathology among early age-of-onset patients with behavioral or language syndromes.

Some studies have suggested greater striatal pathology in FTLD-tau[16] compared to other FTLD subtypes, perhaps correlating with more severe extrapyramidal motor symptoms in these patients. The present study, however, was based on clinical rather than pathological groupings and could not determine whether tau pathology was associated with greater motor system-related striatal injury. Interestingly, the most recently described FTLD subtype, FTLD-FUS[27] is accompanied by severe behavioral derangements and prominent caudate atrophy in vivo[48] and at autopsy. The one patient in this study with bvFTD due to autopsy-confirmed FTLD-FUS showed the most severe overall striatal atrophy of any subject (Figure 2).

4.3. Relationship between striatal atrophy patterns and cortico-striatal connectivity

Human cortico-striatal connectivity has been inferred, for the most part, from animal tracer studies. In monkeys, dorsolateral and dorsomedial frontal cortices project to a central diagonal band of caudate and putamen, while orbitofrontal, anterior cingulate, and temporal polar regions project to the ventromedial caudate-putamen and NAcc[25, 26]. Posterior parietal cortex, in contrast, shows only light projections to a strip of dorsolateral caudate-putamen[49]. These projection fields are organized as longitudinal bands running the antero-posterior length of the striatum. Macaque inferotemporal cortex, homologous to a region heavily affected in SD, provides dense inputs to the NAcc and amygdala[26]. Diffusion tensor imaging and functional connectivity MRI studies suggest that human cortico-striatal networks parallel those seen in monkeys[50–52].

Our findings relate closely to these established striatal connectivity patterns. In bvFTD, a disorder affecting medial and orbital, but also lateral frontal cortex, we found atrophy across all striatal subregions. In SD, which focuses its initial assault on the temporal pole and amygdala[4] before spreading to orbital-insular and medial frontal regions[53], we found severe ventral striatal involvement. These patterns suggest that striatal subregion atrophy proceeds along connectional lines, reflecting a network-based degeneration cascade[8]. In AD, a posterior hippocampal-cingulo-temporo-parietal syndrome, we detected minimal striatal degeneration, perhaps because AD posterior cortical vulnerability follows cortico-cortical[54] and corticolimbic[55], rather than corticostriatal connections. Nonetheless, the mild NAcc atrophy detected in AD may reflect NAcc inputs from the entorhinal/hippocampal regions affected early in AD[56].

5. Limitations

Manual ROI tracing provides the gold standard for volume quantification within structures for which *a priori* hypotheses can be made. This method, however, has two major limitations. First, it is labor intensive, limiting sample size. Although this study confirmed *a priori* predicted between-group differences, more subtle between- and within-group effects may have been detectable with larger samples. Second, ROI volumetrics constrain inferences to those regions chosen for study. Therefore, subtle dorsoventral gradations within the caudate or putamen, for example, would have been missed in this study. In addition, only a subset of our study subjects had standardized prospective motor, behavioral and neuropsychological data available. Finally, matching for disease severity across clinical diagnoses can prove challenging, although the groups selected here showed no statistical differences in CDR, MMSE, or disease duration. Despite these caveats, our observations highlight the importance of striatal degeneration in FTD pathogenesis and symptoms.

6. Future directions

Future translational research could capitalize on the well-conserved organization of striatal circuits in rodents. Some functions lost in bvFTD and SD, such as self-conscious emotion, social cognition, and semantic knowledge, cannot be modeled in transgenic animals. Many aspects of ventral striatal function, however, have been largely conserved from mice to humans. Behavioral phenotypes relevant to human overeating and compulsivity have been produced by rodent genetic manipulations[57, 58], and emerging FTD rodent models could use striatal function as an index of model validity, treatment response, and longitudinal change. Our human data provide an important step toward building this translational interface.

Acknowledgments

We thank the Mental Health Clinical Research Center at the University of Iowa for enabling our use of BRAINS2 software and Jee H. Jeong, Alisa Maitlin, and John Neuhaus for assistance. This study was supported by National Institute on Aging (NIA, grants K08 AG027086, P01 AG19724, P50 AG1657303-75271, and P30 AG10124), National Institute of Neurological Disorders and Stroke (K23 NS408855), the Larry L. Hillblom Foundation, the Consortium for Frontotemporal Dementia Research, and the John Douglas French Alzheimer's Disease foundation. Finally, we thank our patients and their families for participating in dementia research.

References

1. Woolley JD, Gorno-Tempini ML, Seeley WW, et al. Binge eating is associated with right orbitofrontal-insular-striatal atrophy in frontotemporal dementia. Neurology. 2007 Oct 2; 69(14): 1424–33. [PubMed: 17909155]
2. Miller BL, Darby AL, Swartz JR, Yener GG, Mena I. Dietary changes, compulsions and sexual behavior in frontotemporal degeneration. Dementia. 1995; 6(4):195–9. [PubMed: 7550598]

3. Snowden JS, Bathgate D, Varma A, Blackshaw A, Gibbons ZC, Neary D. Distinct behavioural profiles in frontotemporal dementia and semantic dementia. J Neurol Neurosurg Psychiatry. 2001 Mar; 70(3):323–32. [PubMed: 11181853]
4. Seeley WW, Bauer AM, Miller BL, et al. The natural history of temporal variant frontotemporal dementia. Neurology. 2005 Apr 26; 64(8):1384–90. [PubMed: 15851728]
5. Rosso SM, Roks G, Stevens M, et al. Complex compulsive behaviour in the temporal variant of frontotemporal dementia. J Neurol. 2001 Nov; 248(11):965–70. [PubMed: 11757960]
6. Nyatsanza S, Shetty T, Gregory C, Lough S, Dawson K, Hodges JR. A study of stereotypic behaviours in Alzheimer's disease and frontal and temporal variant frontotemporal dementia. J Neurol Neurosurg Psychiatry. 2003 Oct; 74(10):1398–402. [PubMed: 14570833]
7. Rinne JO, Laine M, Kaasinen V, Norvasuo-Heila MK, Nagren K, Helenius H. Striatal dopamine transporter and extrapyramidal symptoms in frontotemporal dementia. Neurology. 2002 May 28; 58(10):1489–93. [PubMed: 12034784]
8. Seeley WW, Crawford RK, Zhou J, Miller BL, Greicius MD. Neurodegenerative diseases target large-scale human brain networks. Neuron. 2009 Apr 16; 62(1):42–52. [PubMed: 19376066]
9. Rosen HJ, Gorno-Tempini ML, Goldman WP, et al. Patterns of brain atrophy in frontotemporal dementia and semantic dementia. Neurology. 2002 Jan 22; 58(2):198–208. [PubMed: 11805245]
10. Boccardi M, Sabattoli F, Laakso MP, et al. Frontotemporal dementia as a neural system disease. Neurobiol Aging. 2005 Jan; 26(1):37–44. [PubMed: 15585344]
11. Whitwell JL, Josephs KA, Rossor MN, et al. Magnetic resonance imaging signatures of tissue pathology in frontotemporal dementia. Arch Neurol. 2005 Sep; 62(9):1402–8. [PubMed: 16157747]
12. Seeley WW, Crawford R, Rascovsky K, et al. Frontal paralimbic network atrophy in very mild behavioral variant frontotemporal dementia. Arch Neurol. 2008 Feb; 65(2):249–55. [PubMed: 18268196]
13. Garibotto V, Borroni B, Agosti C, et al. Subcortical and deep cortical atrophy in Frontotemporal Lobar Degeneration. Neurobiol Aging. 2011 May; 32(5):875–84. [PubMed: 19501427]
14. Looi JC, Walterfang M, Styner M, et al. Shape analysis of the neostriatum in subtypes of frontotemporal lobar degeneration: neuroanatomically significant regional morphologic change. Psychiatry Res. 2011 Feb 28; 191(2):98–111. [PubMed: 21237621]
15. Senjem ML, Gunter JL, Shiung MM, Petersen RC, Jack CR Jr. Comparison of different methodological implementations of voxel-based morphometry in neurodegenerative disease. Neuroimage. 2005 Jun; 26(2):600–8. [PubMed: 15907317]
16. Kim EJ, Rabinovici GD, Seeley WW, et al. Patterns of MRI atrophy in tau-positive and ubiquitin-positive frontotemporal lobar degeneration. J Neurol Neurosurg Psychiatry. 2007 Jul 5.
17. Looi JC, Lindberg O, Zandbelt BB, et al. Caudate nucleus volumes in frontotemporal lobar degeneration: differential atrophy in subtypes. AJNR Am J Neuroradiol. 2008 Sep; 29(8):1537–43. [PubMed: 18782907]
18. Looi JC, Svensson L, Lindberg O, et al. Putaminal volume in frontotemporal lobar degeneration and Alzheimer disease: differential volumes in dementia subtypes and controls. AJNR Am J Neuroradiol. 2009 Sep; 30(8):1552–60. [PubMed: 19497964]
19. Whitwell JL, Sampson EL, Loy CT, et al. VBM signatures of abnormal eating behaviours in frontotemporal lobar degeneration. Neuroimage. 2007 Mar; 35(1):207–13. [PubMed: 17240166]
20. Josephs KA, Whitwell JL, Jack CR Jr. Anatomic correlates of stereotypies in frontotemporal lobar degeneration. Neurobiol Aging. 2007 Jun 13.
21. Kril JJ, Macdonald V, Patel S, Png F, Halliday GM. Distribution of brain atrophy in behavioral variant frontotemporal dementia. J Neurol Sci. 2005 May 15; 232(1–2):83–90. [PubMed: 15850587]
22. Josephs KA, Stroh A, Dugger B, Dickson DW. Evaluation of subcortical pathology and clinical correlations in FTLD-U subtypes. Acta Neuropathol. 2009 Sep; 118(3):349–58. [PubMed: 19455346]
23. Tsuchiya K, Ikeda K. Basal ganglia lesions in 'Pick complex': a topographic neuropathological study of 19 autopsy cases. Neuropathology. 2002 Dec; 22(4):323–36. [PubMed: 12564774]

24. Geser F, Martinez-Lage M, Robinson J, et al. Clinical and pathological continuum of multisystem TDP-43 proteinopathies. Arch Neurol. 2009 Feb; 66(2):180–9. [PubMed: 19204154]
25. Selemon LD, Goldman-Rakic PS. Longitudinal topography and interdigitation of corticostriatal projections in the rhesus monkey. J Neurosci. 1985 Mar; 5(3):776–94. [PubMed: 2983048]
26. Cheng K, Saleem KS, Tanaka K. Organization of corticostriatal and corticoamygdalar projections arising from the anterior inferotemporal area TE of the macaque monkey: a Phaseolus vulgaris leucoagglutinin study. J Neurosci. 1997 Oct 15; 17(20):7902–25. [PubMed: 9315910]
27. Neumann M, Rademakers R, Roeber S, Baker M, Kretzschmar HA, Mackenzie IR. A new subtype of frontotemporal lobar degeneration with FUS pathology. Brain. 2009 Nov; 132(Pt 11):2922–31. [PubMed: 19674978]
28. Mackenzie IR, Neumann M, Bigio EH, et al. Nomenclature and nosology for neuropathologic subtypes of frontotemporal lobar degeneration: an update. Acta Neuropathol. 2010 Jan; 119(1):1–4. [PubMed: 19924424]
29. Mackenzie IR, Neumann M, Baborie A, et al. A harmonized classification system for FTLD-TDP pathology. Acta Neuropathol. 2011 Jul; 122(1):111–3. [PubMed: 21644037]
30. Sampathu DM, Neumann M, Kwong LK, et al. Pathological heterogeneity of frontotemporal lobar degeneration with ubiquitin-positive inclusions delineated by ubiquitin immunohistochemistry and novel monoclonal antibodies. Am J Pathol. 2006 Oct; 169(4):1343–52. [PubMed: 17003490]
31. Grossman M, Wood EM, Moore P, et al. TDP-43 pathologic lesions and clinical phenotype in frontotemporal lobar degeneration with ubiquitin-positive inclusions. Arch Neurol. 2007 Oct; 64(10):1449–54. [PubMed: 17923628]
32. Liu W, Miller BL, Kramer JH, et al. Behavioral disorders in the frontal and temporal variants of frontotemporal dementia. Neurology. 2004 Mar 9; 62(5):742–8. [PubMed: 15007124]
33. Neary D, Snowden JS, Gustafson L, et al. Frontotemporal lobar degeneration: a consensus on clinical diagnostic criteria. Neurology. 1998; 51(6):1546–54. [PubMed: 9855500]
34. McKhann G, Drachman D, Folstein M, Katzman R, Price D, Stadlan EM. Clinical diagnosis of Alzheimer's disease: report of the NINCDS-ADRDA Work Group under the auspices of Department of Health and Human Services Task Force on Alzheimer's Disease. Neurology. 1984; 34(7):939–44. [PubMed: 6610841]
35. Magnotta VA, Harris G, Andreasen NC, O'Leary DS, Yuh WT, Heckel D. Structural MR image processing using the BRAINS2 toolbox. Comput Med Imaging Graph. 2002 Jul-Aug;26(4):251–64. [PubMed: 12074920]
36. Talairach, J.; Tournoux, P. Co-planar stereotaxic atlas of the human brain: 3-Dimensional proportional system; An approach to cerebral imaging. Stuttgart: George Thieme Verlag; 1988.
37. Woods RP, Cherry SR, Mazziotta JC. Rapid automated algorithm for aligning and reslicing PET images. J Comput Assist Tomogr. 1992; 16(4):620–33. [PubMed: 1629424]
38. Harris G, Andreasen NC, Cizadlo T, et al. Improving tissue classification in MRI: a three-dimensional multispectral discriminant analysis method with automated training class selection. J Comput Assist Tomogr. 1999 Jan-Feb;23(1):144–54. [PubMed: 10050826]
39. The National Institute on Aging aRIWGoDCftNAoAsD. Consensus recommendations for the postmortem diagnosis of Alzheimer's disease. Neurobiol Aging. 1997 Jul-Aug;18(4 Suppl):S1–2. [PubMed: 9330978]
40. Chow TW, Izenberg A, Binns MA, et al. Magnetic resonance imaging in frontotemporal dementia shows subcortical atrophy. Dement Geriatr Cogn Disord. 2008; 26(1):79–88. [PubMed: 18617738]
41. Garibotto V, Borroni B, Agosti C, et al. Subcortical and deep cortical atrophy in Frontotemporal Lobar Degeneration. Neurobiol Aging. 2009 Jun 4.
42. Miller, B.; Boone, K.; Mishkin, F.; Swartz, J.; Koras, N.; Kushii, J. Clincial and neuropsychological features of frontotemporal dementia. In: Kertesz, A.; Munoz, D., editors. Pick's Disease and Pick complex. New York: Wiley-Liss; 1998. p. 23-32.
43. Carelli RM. The nucleus accumbens and reward: neurophysiological investigations in behaving animals. Behav Cogn Neurosci Rev. 2002 Dec; 1(4):281–96. [PubMed: 17712985]
44. Rosen HJ, Allison SC, Schauer GF, Gorno-Tempini ML, Weiner MW, Miller BL. Neuroanatomical correlates of behavioural disorders in dementia. Brain. 2005 Nov; 128(Pt 11): 2612–25. [PubMed: 16195246]

45. Snowden J, Neary D, Mann D. Frontotemporal lobar degeneration: clinical and pathological relationships. Acta Neuropathol. 2007 Jul; 114(1):31–8. [PubMed: 17569065]
46. Hodges JR, Davies RR, Xuereb JH, et al. Clinicopathological correlates in frontotemporal dementia. Ann Neurol. 2004 Sep; 56(3):399–406. [PubMed: 15349867]
47. Klunk WE, Price JC, Mathis CA, et al. Amyloid deposition begins in the striatum of presenilin-1 mutation carriers from two unrelated pedigrees. J Neurosci. 2007 Jun 6; 27(23):6174–84. [PubMed: 17553989]
48. Josephs KA, Whitwell JL, Parisi JE, et al. Caudate atrophy on MRI is a characteristic feature of FTLD-FUS. Eur J Neurol. 2010 Jul; 17(7):969–75. [PubMed: 20236174]
49. Selemon LD, Goldman-Rakic PS. Common cortical and subcortical targets of the dorsolateral prefrontal and posterior parietal cortices in the rhesus monkey: evidence for a distributed neural network subserving spatially guided behavior. J Neurosci. 1988 Nov; 8(11):4049–68. [PubMed: 2846794]
50. Lehericy S, Ducros M, Van de Moortele PF, et al. Diffusion tensor fiber tracking shows distinct corticostriatal circuits in humans. Ann Neurol. 2004 Apr; 55(4):522–9. [PubMed: 15048891]
51. Seeley WW, Menon V, Schatzberg AF, et al. Dissociable intrinsic connectivity networks for salience processing and executive control. J Neurosci. 2007 Feb 28; 27(9):2349–56. [PubMed: 17329432]
52. Kelly AM, Di Martino A, Uddin LQ, et al. Development of anterior cingulate functional connectivity from late childhood to early adulthood. Cereb Cortex. 2009 Mar; 19(3):640–57. [PubMed: 18653667]
53. Brambati SM, Rankin KP, Narvid J, et al. Atrophy progression in semantic dementia with asymmetric temporal involvement: A tensor-based morphometry study. Neurobiol Aging. 2007 Jun 29.
54. Giannakopoulos P, Hof PR, Michel JP, Guimon J, Bouras C. Cerebral cortex pathology in aging and Alzheimer's disease: a quantitative survey of large hospital-based geriatric and psychiatric cohorts. Brain Research Brain Research Reviews. 1997; 25(2):217–45. [PubMed: 9403139]
55. Braak H, Braak E. Neuropathological staging of Alzheimer-related changes. Acta Neuropathologica. 1991; 82:239–59. [PubMed: 1759558]
56. Friedman DP, Aggleton JP, Saunders RC. Comparison of hippocampal, amygdala, and perirhinal projections to the nucleus accumbens: combined anterograde and retrograde tracing study in the Macaque brain. J Comp Neurol. 2002 Sep 2; 450(4):345–65. [PubMed: 12209848]
57. Tecott LH. The genes and brains of mice and men. Am J Psychiatry. 2003 Apr; 160(4):646–56. [PubMed: 12668350]
58. Welch JM, Lu J, Rodriguiz RM, et al. Cortico-striatal synaptic defects and OCD-like behaviours in Sapap3-mutant mice. Nature. 2007 Aug 23; 448(7156):894–900. [PubMed: 17713528]

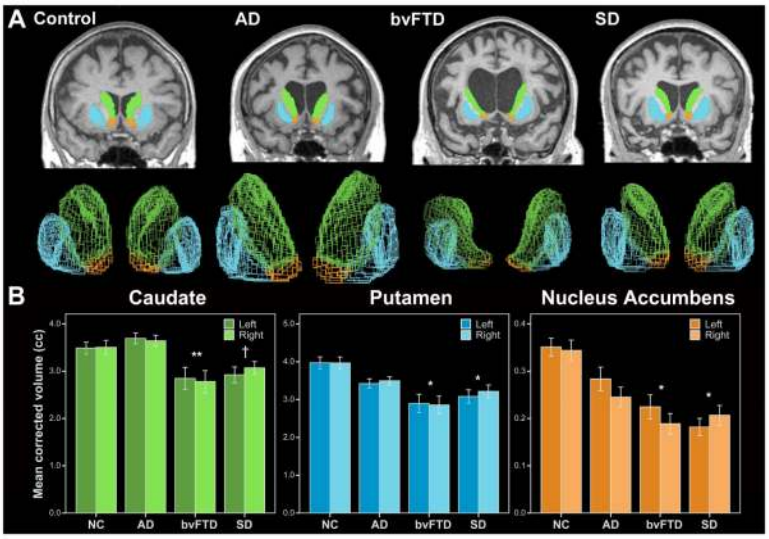

Figure 1. Striatal volume loss in bvFTD and SD

A. ROI tracings and 3D reconstructions of caudate (green), putamen (blue), and nucleus accumbens (orange) from the first supramedian subject in each group. For ease of comparison, images are scaled to the total striatal volume correction factor. **B.** Caudate, putamen, and NAcc volumes (corrected for total intracranial volume) in healthy controls and patients with dementia. Values represent estimated marginal means and bars represent standard error. * = $p < 0.05$ vs. HC; ** = $p < 0.05$ vs. HC and AD; † = $p < 0.05$ vs. AD.

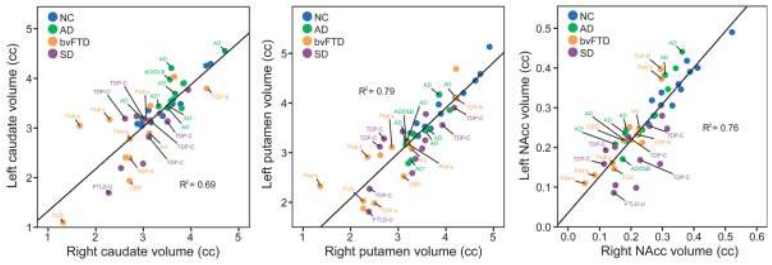

Figure 2. Correlations between left and right striatal volumes

Dots correspond to individual subjects labeled by clinical syndromic diagnosis (color) and histopathology (text label). Pathologic labels are color coded by clinical syndrome and applied to all patients for whom post-mortem diagnosis was available. Severe bilateral striatal atrophy was observed in the patient with FTLD-FUS, as was greater than expected atrophy in one patient with AD due to a presenilin-1 mutation (*) and one with comorbid DLB. A patient with bvFTD due to AD (orange AD label) showed lower striatal volumes than seen in clinically typical AD. FUS = FTLD with FUS immunoreactive inclusions, TDP-A, TDP-B, and TDP-C refer to FTLD with TDP-43 immunoreactive inclusions, Types AC, respectively (Mackenzie et al 2011 scheme).

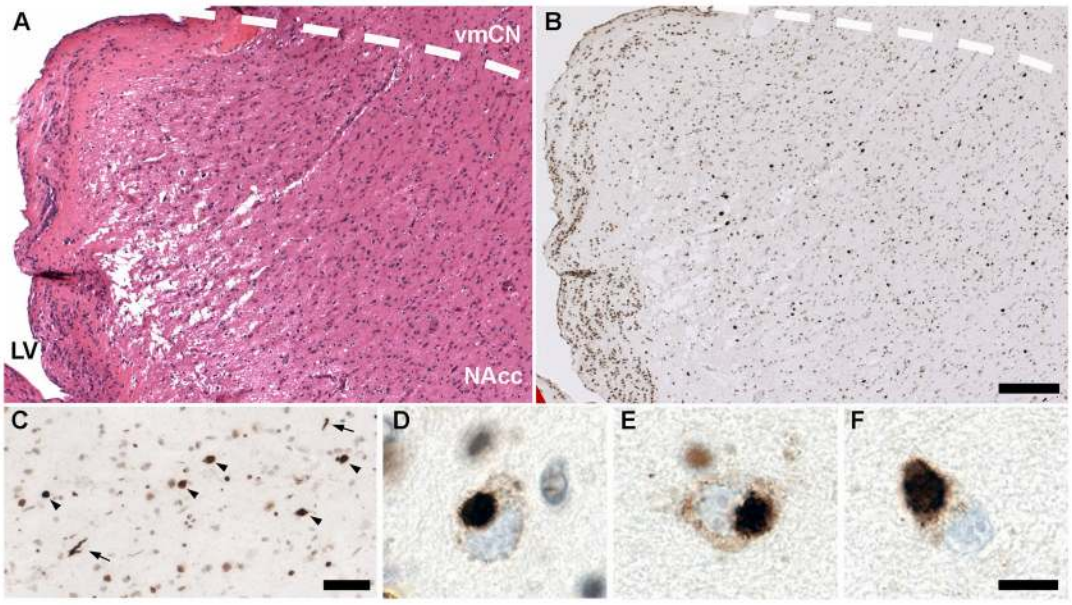

Figure 3. Nucleus accumbens degeneration and TDP-43 pathology in SD

Patients with SD due to FTLD-TDP, Type C showed severe ventral striatal astrogliosis, vacuolation, and neuron loss **(A)** and conspicuous TDP-43 pathology **(B–F)**, manifesting as large, round, circumscribed (Pick body-like) NCIs (arrowheads in **C**) associated with scarce DNs (arrows in **C**). These NCIs were uniformly associated with loss of normal nuclear TDP-43 immunoreactivity **(D–F).** Dotted lines in **A–B** indicate approximate dorsal NAcc border. Scale bar in **B** applies to **A–B** and represents 200 microns. Scale bar in **C** represents 50 microns. Scale bar in **F** applies to **D–F** and represents 10 microns. Hematoxylin and eosin **(A)** and TDP-43 immunohistochemistry with hematoxylin counterstain **(B–F)**. LV = lateral ventricle, NAcc = nucleus accumbens.

Table 1

Group demographic and neuropsychological variables.

	HC	AD	bvFTD	SD	Overall ANOVA
Age at MRI (yrs)	60.1 (5.5)	63.8 (12.7)	61.3 (6.4)	62.3 (6.7)	$F(3, 44) = 0.44$, n.s.
Gender (M:F)	7:5	6:6	7:5	8:4	$\chi^2(3, 44) = 0.69$, n.s.
Education (yrs)	17.0 (3.5)	16.6 (3.4)	15.7 (2.9)	16.9 (2.4)	$F(3, 44) = 0.47$, n.s.
CDR (no, 0/0.5/1/2)	12/0/0/0	0/3/5/2	0/1/8/1	1/4/1/3	$\chi^2(2, 26) = 10.2$, n.s.
MMSE (max = 30)	29.6 (0.5)	20.4 (6.2)	23.8 (6.5)	21.9 (6.6)	$F(2, 33) = 0.85$, n.s.
Disease Duration (yrs)	--	4.8 (2.7)	6.5 (3.6)	5.2 (3.0)	$F(2, 33) = 1.0$, n.s.

Values listed are mean (SD). For CDR, MMSE, and disease duration, only patient groups were compared statistically. M = male, F = female, n.s. = not significant.

Alzheimer Dis Assoc Disord. Author manuscript; available in PMC 2014 January 01.

Table 2

Correlations between striatal volumes and behavior in AD, bvFTD, and SD.

		Euphoria		Apathy		Disinhibition		Aberrant Motor		Eating		NPI Total	
		r	p	r	p	r	P	r	p	r	p	r	p
Caudate	**L**	−0.198	0.2	−0.104	0.3	−0.220	0.2	−0.273	0.1	0.066	0.40	−0.175	0.2
	R	−0.176	0.2	−0.458	0.02 *	−0.393	0.04 *	−0.498	0.01 *	−0.301	0.09	−0.478	0.01 *
Putamen	**L**	−0.048	0.4	−0.116	0.3	−0.155	0.3	−0.378	0.05 *	0.056	0.40	−0.179	0.2
	R	−0.304	0.1	−0.422	0.03 *	−0.496	0.01 *	−0.600	0.002 **††	−0.268	0.10	−0.531	0.007 **†
Nucleus Accumbens	**L**	−0.142	0.3	−0.233	0.2	−0.265	0.1	−0.194	0.2	−0.160	0.20	−0.250	0.1
	R	−0.309	0.1	−0.405	0.03 *	−0.405	0.03 *	−0.294	0.1	−0.396	0.04 *	−0.443	0.02 *
Total Striatum	**L**	−0.139	0.3	−0.134	0.3	−0.218	0.2	−0.361	0.05	0.052	0.40	−0.206	0.2
	R	−0.284	0.1	−0.495	0.01 *	−0.507	0.01 *	−0.611	0.002 **†	−0.329	0.07	−0.571	0.003 **†

* $p < 0.05$ (uncorrected),

** $p < 0.008$ (Bonferroni-corrected for multiple comparisons),

† $p < 0.05$ after controlling for diagnosis,

†† $p < 0.05$ after controlling for diagnosis and TCV.